Two-dimensional Hexagonal Photonic Crystals in the X-band

by

Muhammad Rehan Chaudhry

A Thesis Submitted to the
Graduate School of Sciences and Engineering
in Partial Fulfillment of the Requirements for
the Degree of

Master of Science

in

Optoelectronics and Photonics Engineering

Koç University

September 2015

Koç University

Graduate School of Sciences and Engineering

This is to certify that I have examined this copy of a master's thesis by

Muhammad Rehan Chaudhry

and have found that it is complete and satisfactory in all respects,
and that any and all revisions required by the final
examining committee have been made.

Committee Members:

_____

Ali Serpengüzel, Ph. D. (Advisor)

_____

Özgür Müstecaplıoğlu, Ph. D.

_____

Selçuk Aktürk, Ph. D.

Date: _____

ABSTRACT

Photonic crystals have been a hot area of scientific and technological research, since their proposal in 1987. Photonic crystals are generally known as the “semiconductors” of photonics, and found applications in photonic circuits, optical imaging, and telecommunications. The scope of this research is to study microwave transmission response of 2D hexagonal photonic crystals of graphite rods. We used graphite rods to fabricate a photonic crystal structure and stacked the rods together to form a hexagonal lattice. In order to characterize the structure, we measured the transmission of the photonic crystal in the microwave X-band. No structure is observed in the transverse electric (TE) polarization transmission spectrum, as the graphite rods absorb more efficiently for that geometry. A photonic band gap with a width of 0.5 GHz is observed for transverse magnetic (TM) polarization at 10.8 GHz. As the angle of incidence is scanned, we observed the shifting of the bandgap frequency. A similar bandgap frequency was observed at 0^0 and 60^0 coinciding with the symmetry of the photonic crystal. We induced defect states in the photonic crystal, and observed a mode in the band gap, for a point defect. As Maxwell’s equations are scalable, we can scale down our hexagonal photonic crystal to operate in micro to nano length scales. Our results show that, 2D graphite photonic crystals can be useful in microwave engineering.

ÖZET

1987de ortaya atılmalarından sonra, fotonik örütler son yıllarda büyük ilgi görmeye başlamış bilimsel ve teknolojik bir araştırma konusudur. Fotonik örütler, optiğin "yarıiletkenleri" olarak sunulmuş, ve fotonik devreler, optik görüntüleme, ve iletişim alanlarında kullanılmıştır. Bu çalışmada, grafit çubuklardan oluşan 2 boyutlu fotonik örüt yapısının mikrodalga geçirgenliği incelenmiştir. Grafit çubuklar altıgen örgü yapısında bir araya getirilerek bir fotonik örüt yapılmıştır. Grafit fotonik örüt yapısının incelenmesi amacıyla, X-bandında geçirgenlik ölçümleri gerçekleştirilmiştir. Grafit çubuklar bu geometride soğurduğu için, enine elektrik (TE) kutuplama geçirgenlik izgesinde bir im görülmemiştir. Enine manyetik (TM) kutuplama için 10.8 GHz sıklığında 0.5 GHz genişliğinde bir yasak bant aralığı gözlemlenmiştir. Fotonik örüte gönderilen mikrodalganın geliş açısına göre yasak bant aralığında bir değişim gözlemlenmiş, ve 0^o ile 60^o açıları için aynı yasak bant aralığı ölçülmüştür. Bu sonuç altıgen örgülü grafit örütün doğal yapısıyla uyum göstermektedir. Ek olarak, fotonik örüt yapısında noktasal örgü bozukluğu oluşturulmuş, ve ölçülen sıklıklarda bir kip gözlemlenmiştir. Maxwell denklemleri ölçeğe göre ayarlanabilir olduğundan, altıgen fotonik örüt yapısının mikro ve nano boyutlarda da çalışabileceğini öngörmekteyiz. Elde edilen sonuçlara göre, 2 boyutlu grafit fotonik örüt yapılarının mikrodalga alanında yararlı olacağı beklenmektedir.

ACKNOWLEDGEMENTS

I would like to express my gratitude to my supervisor, Prof. Dr. Ali Serpengüzel for providing me opportunity to begin research in his group at Koç University Microphotonics Research Laboratory (KUMRL) and for his constant guidance, understanding, and patience during my Master's degree study in Koç University. I would also like to thank my committee members Prof. Dr. Özgür Müstecaplıoğlu, and Assoc. Prof. Dr. Selçuk Aktürk for their reading of my thesis and their constructive comments.

I would also like to thank research group members, namely Dr. Ulaş Sabahattin Gökay (Post-Doctoral Research Associate), Muhammad Sohail Anwar (MSc), Muhammad Hamza Humayun (MSc), Imran Khan (MSc), Syed Sultan Shah Bukhari (MSc), and especially Zeeshan Rashid (PhD), Muhammad Zakwan (PhD), and Farhan Azeem (MSc) for their help in experimental setup, figures and moral boosting. It was really an honor to part of such wonderful team.

Coursework at Koç University helped me a lot in my research, especially homeworks and assignments by Assist. Prof. Dr. Şükrü Ekin Kocabaş.

Moving forward, I would like to thank Assoc. Prof. Dr. Kaan Güven for granting access to his laboratory and the network analyzer for recording experimental data and Koç University Optical Microsystems Laboratory (OML) for lending the 360^0 rotation stage.

Finally, I would thank Pakistan Higher Education Commission (HEC) for all the financial support, which could make this study a reality.

To my parents

Table of Contents

List of Figures

NOMENCLATURE

a	Lattice constant
c	Speed of light in vacuum
d	Diameter of rods
$\varepsilon(r)$	Dielectric Constant
ε_0	Dielectric constant in free space
k	Propagation vector
r	Radius of rods
λ	Wavelength of light in vacuum
μ_0	Vacuum Permeability
ω	Angular frequency
Θ	Hermitian Operator
D	Electrical Displacement
B	Magnetic induction
$E_\perp$	Perpendicular electric field
$E_\parallel$	Parallel electric field
$H_\perp$	Perpendicular magnetic field
$H_\parallel$	Parallel magnetic field
Γ	Wavevector origin in reciprocal space
M	Wavevector direction in reciprocal space
K	Wavevector direction in reciprocal space
X	Wavevector direction in reciprocal space

Chapter 1

INTRODUCTION

1.1 Photonic Crystals

Natural scientists and engineers have been working for years to control optical properties of materials. One of the most fruitful products of this hard work is the optical fiber, which has revolutionized the data transferring speeds in telecommunications. Optical fiber molds the flow of light through a dielectric core using the law of reflection [1]. Photonic crystals (PCs) have also been a hot area of research, because of their property to guide light. PCs were first proposed in 1987 by Eli Yablonovitch and Sajeev John [2] [3]. Electromagnetic (EM) wave propagation in periodic dielectric structure is a similar process, to electron waves propagating in a crystal. An analogy can be drawn between both crystals, as there is an energy band in conventional crystals to prevent the movement of electrons, and similarly photonic crystals control the propagation of EM waves [4]. Photonic crystals (PCs) are composed of materials stacked together such that, the dielectric constant ε is changing in a periodic manner. Due to such periodic arrangement of dielectric constant, PCs reflect electromagnetic waves ,which fall in the forbidden frequency range called as the band gap (BG) [5], EM waves within this frequency range cannot propagate through the photonic crystal [6] and are reflected [7].

Similar phenomenon happens in semiconductor electronics, where the bandgap is the narrow zone of energies, which electrons cannot occupy [8]. This property of photonic crystals to mold the flow of light has developed lots of interest, and increased research in this area [9]. Semiconductor materials are available in nature, whereas photonic crystals are manufactured artificially, although some examples are also found in nature at the wings of butterflies, feathers of peacocks, and in opals [10].

Electromagnetic wave propagation in periodically changing dielectric medium is analogous to electron wave propagation in crystals. In solid state physics, solutions of energy as a function of wave vector known as band structures are solved by Schrödinger equation, and in electromagnetics wave solutions are obtained by solving Maxwell's equations.

Figure 1.1(a) shows the simplest case, in which two materials X and Y are stacked together, and the periodic distance between the two identical materials is denoted by *a*,

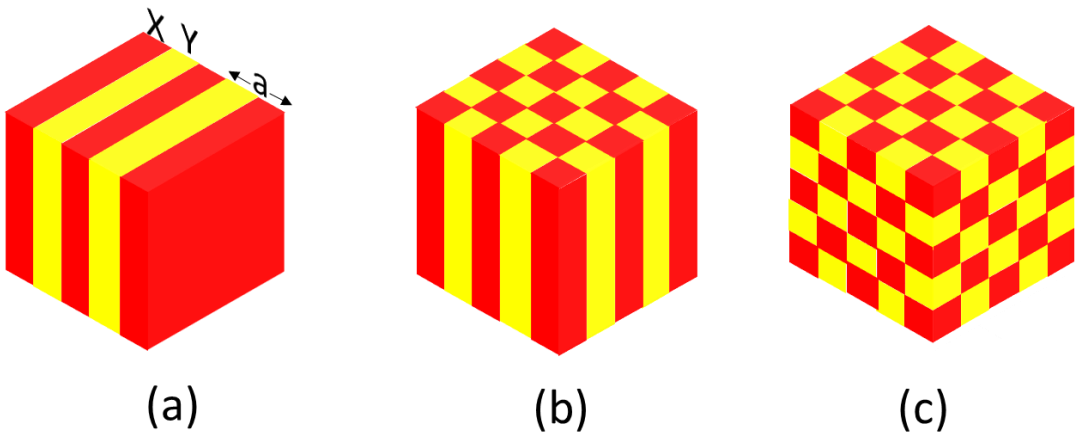

Figure 1.1: (a) 1 D, (b) 2D, (c) and 3D photonic crystal.

which is also called lattice constant (as in the case of ordinary crystals). There are many similarities between the photonic crystals and ordinary crystals [11], but the main difference is the scale of lattice constant. In ordinary crystals the lattice constant is of the scale of the electromagnetic wave. The lattice constant is in cm for microwave frequencies and less than one μm for visible light.

In solid state physics, crystals offer a periodic potential to the electrons propagating through the crystals. Due to Bragg diffraction from the atoms in the crystal structure, a gap opens up in the allowed energies, which propagating electrons cannot occupy. In a photonic crystal, the periodic potential is provided by the periodic arrangement of the low and the high dielectric constant materials. Bragg scattering from the dielectric structures can produce the same effect as in case of atomic crystals, if the dielectric difference between the stacked materials is high enough [12] [13]. Defects produced in the photonic crystal break the periodicity of the photonic crystal, and modes can be generated in the band of forbidden frequencies [14] [15]. The properties of these modes depend on the type of the defect, i.e., point defect can form a microcavity [16], and a line defect can act as a waveguide [17]. These structures open up new paths to control the flow of light in photonic crystals.

Photonic crystals are mainly divided into three types such as 1D, 2D and 3D photonic crystals as shown in figure 1.1. The idea of 1D periodic dielectric structure dates back to 1887, when Lord Rayleigh discussed in his paper entitled "The Propagation of Waves through a Medium Endowed with a Periodic Structure," the formula for a bandgap [18]. The ideas of 1D laminated mirrors is extended further, and the Bragg mirror has been

studied for a long time [19], before it was introduced that, a bandgap could be observed in more than one dimension [20]. The most common example of 2D photonic crystals is the photonic crystal fiber [21]. 3D photonic crystals also have a bandgap and can mold the flow of light in all directions, but their fabrication is a challenging task [22].

A two dimensional photonic crystal has a dielectric constant varying in two dimensions, while the dielectric constant remains constant in the third dimension [23]. The simple example, we can consider, is a square lattice of dielectric rods in air, as shown in Figure 1.2. For some values of distance between dielectric rods, there can be photonic band gap in the xy plane and in that gap all the incident light is reflected.

1.2 Bragg Scattering

Properties of photonic crystals are due to the interference phenomenon known as Bragg scattering [24]. Bragg reflections from layered periodic structure has been studied, where crystal planes behave as Bragg mirror, if condition $m\lambda = 2a\cos\theta$ is satisfied, where

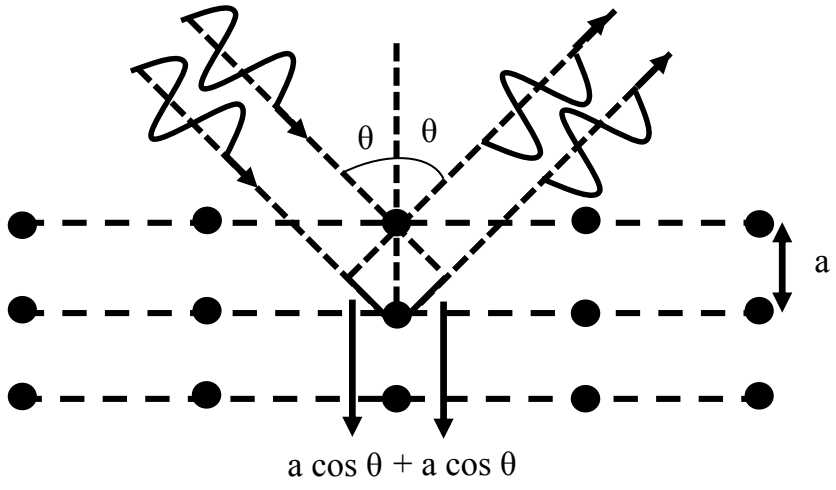

Figure 1.2: Lattice planes spaced by ‘a’ constructively reflect an incident wave.

θ is the angle of incident photons make with the normal, and *a* the distance between the planes. Light is reflected due to constructive interference, when the path difference $2a\cos\theta$ is equal to the integer multiple of wavelength. It can be also deduced that, reflection is wavelength dependent, which gives rise to distinct appearance of photonic crystals. Reflection is 100% for a pure periodic crystal. Let us consider the example of 1D slab with a dielectric constant. Eigen solutions for the PC with a constant dielectric are $\omega(k) = ck/\sqrt{\varepsilon}$. The resulting dispersion relation is of unbounded, but periodic, as per Bloch theorem. Dispersion relation of 1D structure with $\varepsilon_1<\varepsilon_2$ is represented in Figure 1.3 (b), which shows the splitting of the original state into two states with an angular frequency gap of Δω.

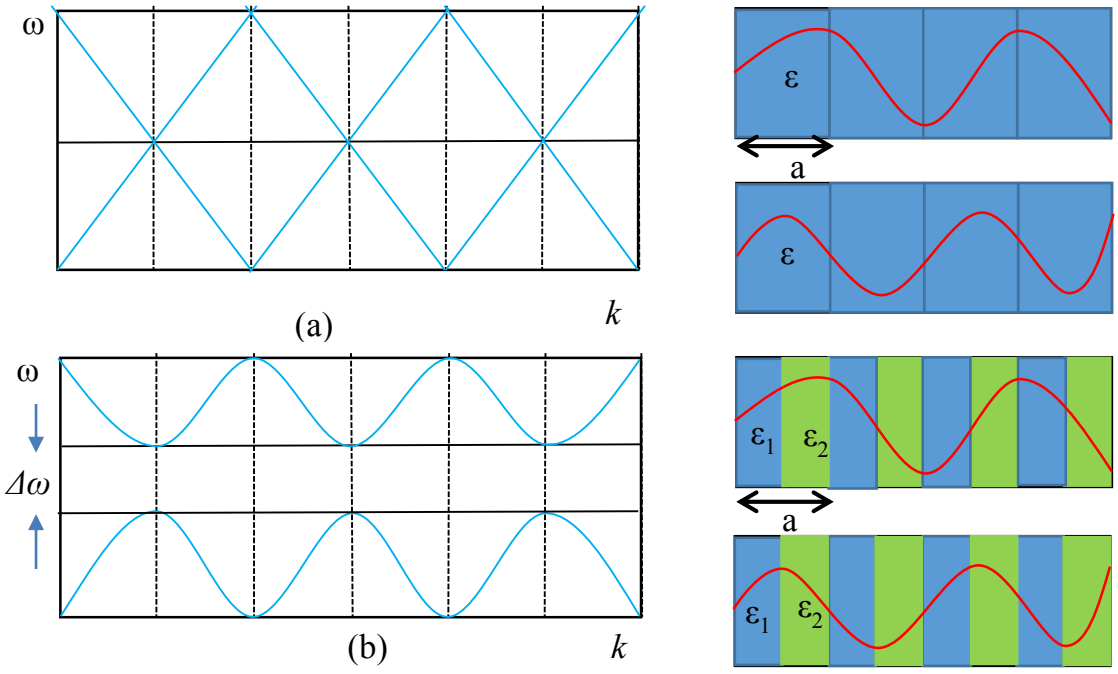

Figure 1.3: Dispersion curve of a lattice with (a) ε and (b) $\varepsilon_1<\varepsilon_2$.

The angular frequency bandgap $\Delta\omega$ varies with the difference in refractive indices of two materials, if the difference is high, we can observe a large photonic bandgap. Small photonic bandgaps are observed for small difference in refractive indices. Probing more into the dispersion relationship, we can observe the same frequency values, when k difference equals to $2\pi/a$, which shows the redundancy in calculations and to avoid it, one should work with the reduced Brillouin zone [25].

1.3 Thesis Structure

This thesis is divided into five chapters. In Chapter 1, the introduction to photonic crystal is provided. Chapter 1 briefly discusses how photonic crystals respond to EM waves propagating through the dielectric medium.

Chapter 2 gives a brief mathematical explanation of the EM waves propagating through the medium and the relevant theory to understand the crystal lattices.

In Chapter 3, a brief introduction to free FDTD simulation package MPB (MIT photonic bands) is provided, and a band diagram of a hexagonal structure is plotted.

Chapter 4 deals with the experimental setup and the first series of experiment, we performed to analyze the rotation symmetry of the PC structure. Later experimental work is further proceeded, and presence of defects in PCs is discussed. Mode occurrence, because of defects is discussed.

Chapter 5 concludes the work, and gives insight into future experimental work.

Chapter 2

THEORETICAL BACKGROUND

2.1 Maxwell's Equations

To study the propagation of light in photonic crystals, we can start by writing Maxwell's equations:

$$\nabla . D(r,t) = 0 \qquad (2.1),$$

$$\nabla . B(r,t) = 0 \qquad (2.2),$$

$$\nabla \times E(r,t) = -\frac{\partial}{\partial t} B(r,t) \qquad (2.3),$$

$$\nabla \times H(r,t) = \frac{\partial}{\partial t} D(r,t) \qquad (2.4),$$

where *E* represents the electric field, *H* the magnetic field, *D* the electrical displacement, and *B* the magnetic induction. Equation (2.3) is called the Faraday's law, and it describes how a time varying magnetic field can induce an electric field. Equation (2.4) is called the Ampere's Law, and it describes magnetic field induction due to time varying electric flux. The relationships between D, E and B, H are written as:

$$B = \mu_0 H \quad (2.5),$$

$$D = \varepsilon_0 \varepsilon(r) E \quad (2.6),$$

In (2.5), $\mu_0 = 4\pi \times 10^{-7}$ Henry/m is the vacuum permeability (we have assumed μ(r), relative permeability to be 1). Putting the values of (2.5) and (2.6) in equations (2.1 – 2.4) will yield the following results:

$$\nabla.[\varepsilon_0 \varepsilon(r) E(r,t)] = 0 \quad (2.7),$$

$$\nabla.[\mu_0 H(r,t)] = 0 \quad (2.8),$$

$$[\nabla \times E(r,t)] = -\frac{\partial}{\partial t}[\mu_0 H(r,t)] \quad (2.9),$$

$$\nabla \times H(r,t) = \frac{\partial}{\partial t}[\varepsilon_0 \varepsilon(r) E(r,t)] \quad (2.10),$$

Taking the curl of both sides of (2.9) gives:

$$\nabla \times [\nabla \times E(r,t)] = -\mu_0 \frac{\partial}{\partial t}[\nabla \times H(r,t)] \quad (2.11).$$

Solving to eliminate H(r,t) from above equation results in:

$$\nabla \times [\nabla \times E(r,t)] = -\mu_0 \varepsilon_0 \varepsilon(r) \frac{\partial^2}{\partial t^2} E(r,t)$$

$$\frac{1}{\varepsilon(r)} \nabla \times [\nabla \times E(r,t)] = -\frac{1}{c^2} \frac{\partial^2}{\partial t^2} E(r,t) \quad (2.12).$$

Similarly, we can eliminate E(r,t) from (2.10) and write it as:

$$\nabla \times [\frac{1}{\varepsilon(r)} \nabla \times H(r,t)] = -\frac{1}{c^2} \frac{\partial^2}{\partial t^2} H(r,t) \quad (2.13),$$

where $c = 1/\sqrt{\mu_0 \varepsilon_0}$.

2.2 Eigenvalue Problem

We can write a solution of (2.11) and (2.12) as:

$$H(r,t) = H(r)e^{-i\omega t}$$

$$E(r,t) = E(r)e^{-i\omega t} \qquad (2.14).$$

Substituting (2.14) into (2.9) and (2.10), we get:

$$\nabla \times E(r,t) = -\frac{\partial}{\partial t}\mu_0 H(r)e^{-i\omega t}$$

$$\nabla \times E(r) = i\omega\mu_0 H(r)$$

$$H(r) = \frac{-i}{\omega\mu_0}\nabla \times E(r) \qquad (2.15).$$

Similarly, we can write for E(r) the following:

$$\nabla \times H(r,t) = \frac{\partial}{\partial t}\varepsilon_0 \varepsilon(r) E(r)e^{-i\omega t}$$

$$\nabla \times H(r) = -i\omega\varepsilon_0 \varepsilon(r) E(r)$$

$$E(r) = \frac{i}{\omega\varepsilon_0 \varepsilon(r)}\nabla \times H(r) \qquad (2.16).$$

Taking the curl of (2.16) gives:

$$\nabla \times E(r) = \frac{i}{\omega \varepsilon_0 \varepsilon(r)} [\nabla \times \nabla \times H(r)] \quad .$$

Substituting the value of curl of E in (2.15) results in:

$$H(r) = \frac{-i}{\omega \mu_0} \frac{i}{\omega \varepsilon_0} \nabla \times [\frac{1}{\varepsilon(r)} \nabla \times H(r)]$$

$$H(r) = \frac{1}{\omega^2 \mu_0 \varepsilon_0} \nabla \times [\frac{1}{\varepsilon(r)} \nabla \times H(r)]$$

$$\nabla \times [\frac{1}{\varepsilon(r)} \nabla \times H(r)] = (\frac{\omega^2}{c^2}) H(r) \qquad (2.17).$$

If we can find the value of H(r) from the above equation, we can substitute that value of H(r) in (2.16) to find E(r). The above equation can be written as eigenvalue equation in the following form:

$$\Theta H(r) = (\frac{\omega}{c})^2 H(r) \quad ,$$

where

$$\Theta H(r) = \nabla \times [\frac{1}{\varepsilon(r)} \nabla \times H(r)] \quad .$$

By solving equation (2.17), we can find the eigenvectors corresponding to the spatial patterns of the harmonic modes. The eigenvalues are proportional to the squared frequencies of those modes. Θ is a linear and Hermitian operator. Equation (2.17) is the master equation in electromagnetics, and solutions of H(r) and ω depend strongly on

the properties of ε(r). In a perfect photonic crystal, such that ε(r) is alternating in a perfect periodic manner, solutions are determined by wave vector *k*. The region, in which wave vectors can travel, is called the Brillouin zone, and the complete picture of all solutions is called the band structure.

2.3 Photonic Crystal Lattice

The periodicity in the structure of the crystals was first observed in 1912 due to diffraction of x-rays from crystals. The diffraction from the crystals helped in decisively proving that crystals are composed of periodic arrays of atoms.

2.3.1 Primitive and Lattice Vectors

A 2D crystal representing a repetition of identical atoms is shown in Figure 2.1. The lattice represented is keeping its periodicity in x and y directions. It can be said that, this lattice possesses translational symmetry such that, if represented by any vector joining two atoms, the representation will remain same at any point, and it will remain invariant.

If we replace the atoms of the crystals with points representing atoms at equilibrium, then we can form the lattice of the crystal. The lattice is represented by translation vectors. Any point in the lattice can be represented by the position vector as:

$$\mathbf{A} = u_1\mathbf{a_1} + u_2\mathbf{a_2} \quad ,$$

where $\mathbf{a_1}$ and $\mathbf{a_2}$ are two primitive vectors. The shortest vectors joining two adjacent unit cells, and u_1 and u_2 are two integers. **A** defined by two primitive vectors is called the lattice vector, and all the vectors satisfying the above equations are lattice vectors.

2.3.2 Unit Cell

The area covered by the unit vectors $\mathbf{a_1}$ and $\mathbf{a_2}$ constitutes a unit cell such that, if we move this unit cell, we can generate all points on the lattice. The unit cell of the square lattice is shown in green color in Figure 2.1.

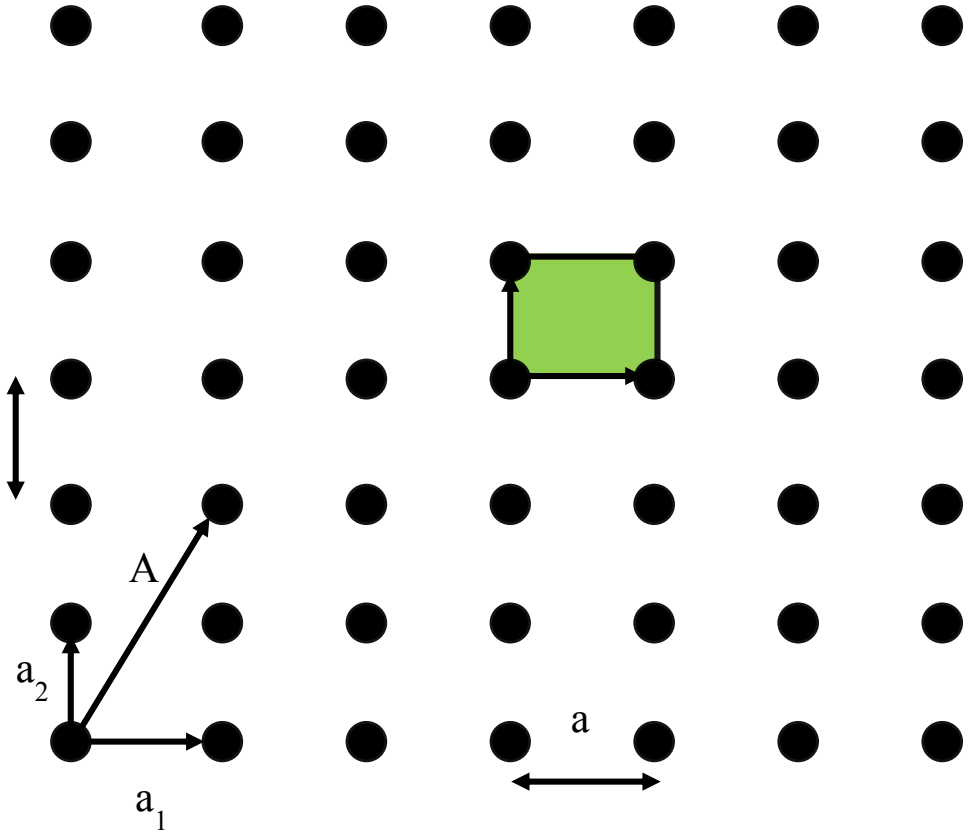

Figure 2.1: Representation of a square lattice.

2.3.3 Bravais and non-Bravais Lattices

Lattices are of two types: *Bravais* and *non-Bravais* lattice. In a Bravais lattice, the structure of lattice remains the same, if it is observed from any point in the lattice. The crystal lattice shown in Figure 2.1 is a Bravais lattice, as the crystal structure remains the same, and we can find atoms at equivalent distance from any observing point. There are five possible Bravais lattices in 2D, as shown in Figure 2.2.

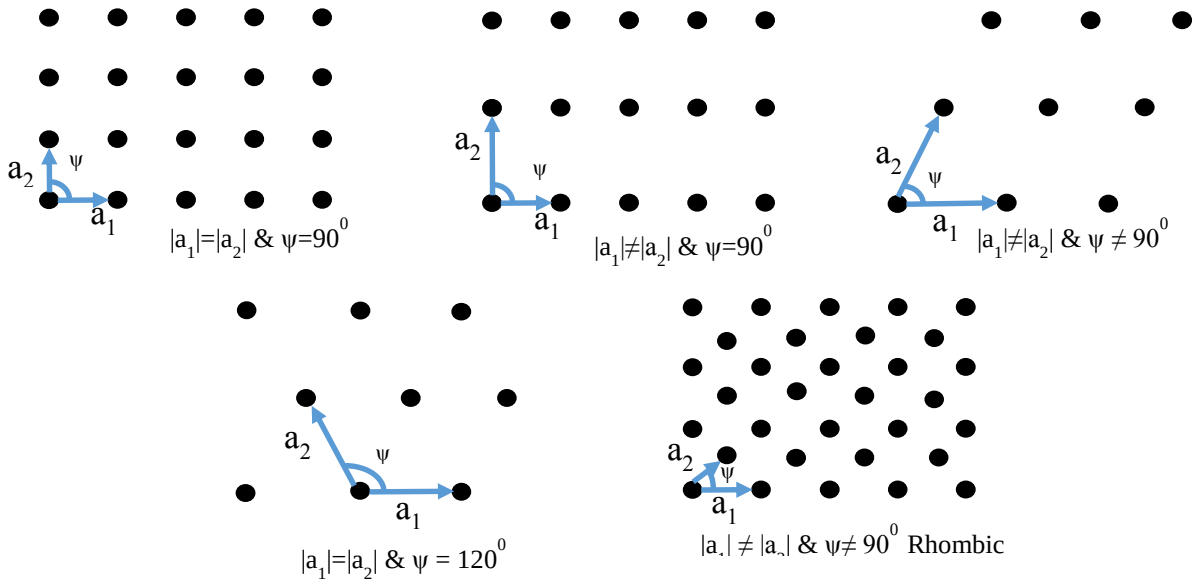

Figure 2.2: 2D Bravais Lattices.

A non-Bravais lattice example is shown in figure 2.3, and we can observe that the environment experienced by the red atom 1 is different from the environment experienced by the blue atom 2.

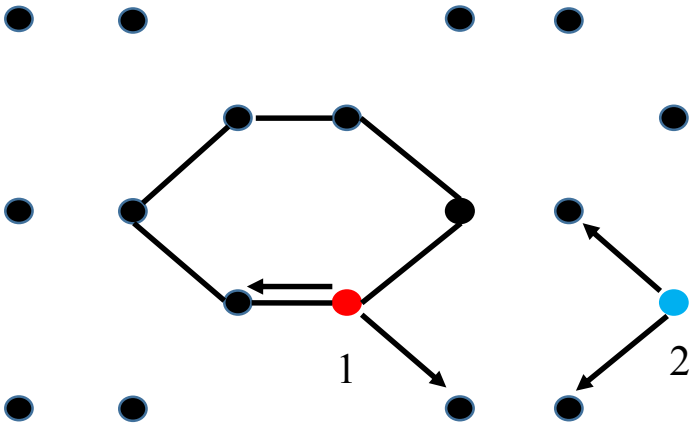

Figure 2.3: Non Bravais honeycomb lattice.

2.3.4 Reciprocal Lattice

The reciprocal lattice is used to represent the crystal structure. The crystal planes and the axes are in a different framework than the real lattice. The dimensions of the reciprocal lattice are 1/length similar to that of the k vector, which is also in the dimension of 1/length. The concept of reciprocal space was introduced by crystallographer named Ewald. The need of reciprocal lattice arose to understand the results of the X-ray diffraction. X-ray diffraction do not tell us the position of atoms in real space, it shows us the Bragg peaks scattered from the crystal in various directions and positions [26]. Only the angle of the point and its intensity are known. Each Bragg point obtained from X-ray diffraction can be represented by Miller indices (hkl) and is plotted in a lattice, which has a reciprocal relation with real lattice. Reciprocal lattice is mainly used to plot the diffraction points, and to get information about the real lattice,

but is also more convenient to solve crystal properties, and electronic structure problems in reciprocal lattice, as compared to real lattice.

A real cubic lattice in three dimensions can be represented by three unit vectors **a1**, **a2** and **a3**.Then the reciprocal lattice can be represented by unit vectors **b1**, **b2** and **b3**, and their relation with real space unit vectors is

$$b_1 = 2\pi \frac{a_2 \times a_3}{V},\ b_2 = 2\pi \frac{a_3 \times a_1}{V} \text{ and } b_3 = 2\pi \frac{a_1 \times a_2}{V} \qquad (2.18),$$

where V is the volume of unit cell in real lattice with $V = \left| a_1 \cdot \left(a_2 \times a_3 \right) \right|$ [27].

It can be deduced from the above relations that the reciprocal primitive vectors have one vector quantity, which is orthogonal to the plane of the vectors involved in the cross product. In case of **b1**, the direction of **b1** is orthogonal to the plane containing **a2** and **a3** vectors.

So the reciprocal primitive lattice vectors have the property $b_i.a_j = 2\pi\delta_{ij}$, where δ_{ij} is the Kronecker delta function, and its value equals to 1, when *i=j*, and equals to 0 otherwise.

The reciprocal lattice vector can be defined in terms of reciprocal primitive vectors as

$$G = v_1 b_1 + v_2 b_2 + v_3 b_3 \qquad (2.19),$$

where v_1, v_2 and v_3 are integers.

2.3.5 Wigner-Seitz Cell

The Wigner-Seitz cell is defined as region in space, which is closer to the specific lattice point than to any other point. A 5x5 square lattice is shown in the following figure and in order to find the region around the red central point, that is closer to central point than to any other point. First of all, we need to identify the neighbors of this point, and need to join the central red point to its neighbors, as shown in the figure 2.4. To find out the midpoint of the lines joining the central point to the neighboring points, and to draw

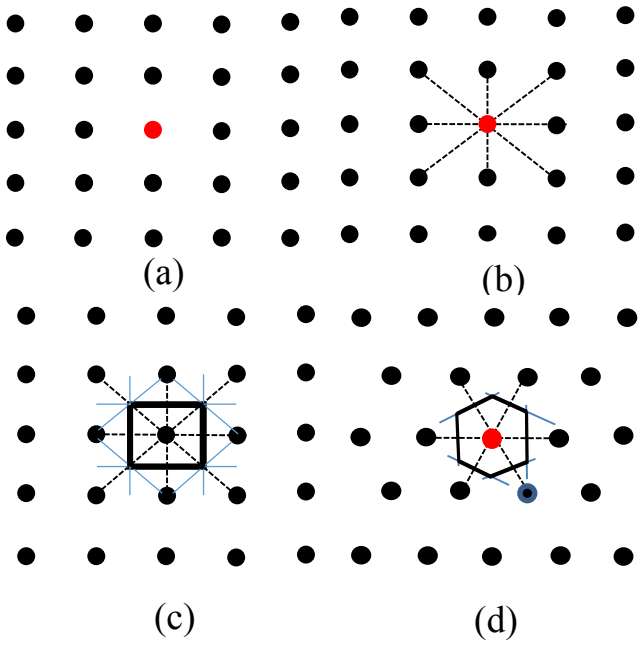

Figure 2.4: (a) lattice, (b) neighbors, (c) and, (d) bisectors and Wigner-Seitz cells.

the perpendicular bisectors. The intersection of the bisectors form a square region around the central point, and points in this region are closer to central point than to any other point in lattice, so, this final square is the Wigner-Seitz cell [28].

2.3.6 Brillouin Zone

The Brillouin zone is defined as the Wigner-Seitz cell in the reciprocal space. The Brillouin zones for square and hexagonal lattice are shown in figure 2.5 (a) and (b).

(a)2-D Square Lattice

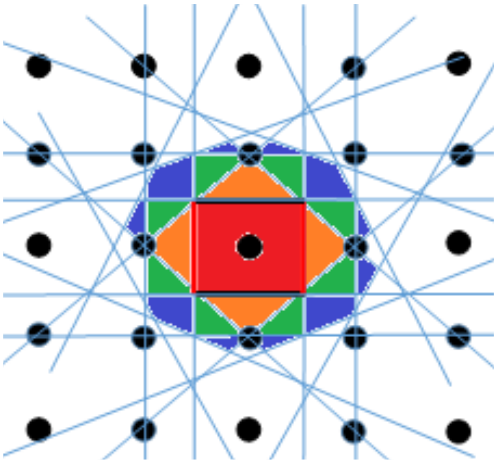

(b) 2-D Hexagonal Lattice

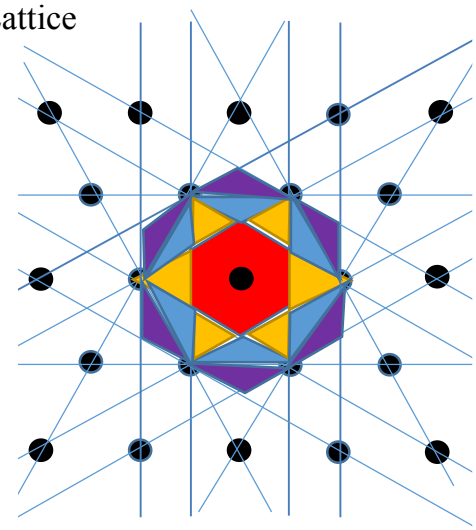

Figure 2.5: Four Brillouin zone regions of 2D (a) square and (b) hexagonal lattice.

First Brillouin zones and irreducible Brillouin zones of square and hexagon lattice are shown in figure 2.6. The irreducible Brillouin zone for both the square and hexagonal lattices is triangular. This is the smallest region of the complete Brillouin zone bounded by the symmetry such that, every point of the Brillouin zone can be constructed from a k-point within the irreducible Brillouin zone.

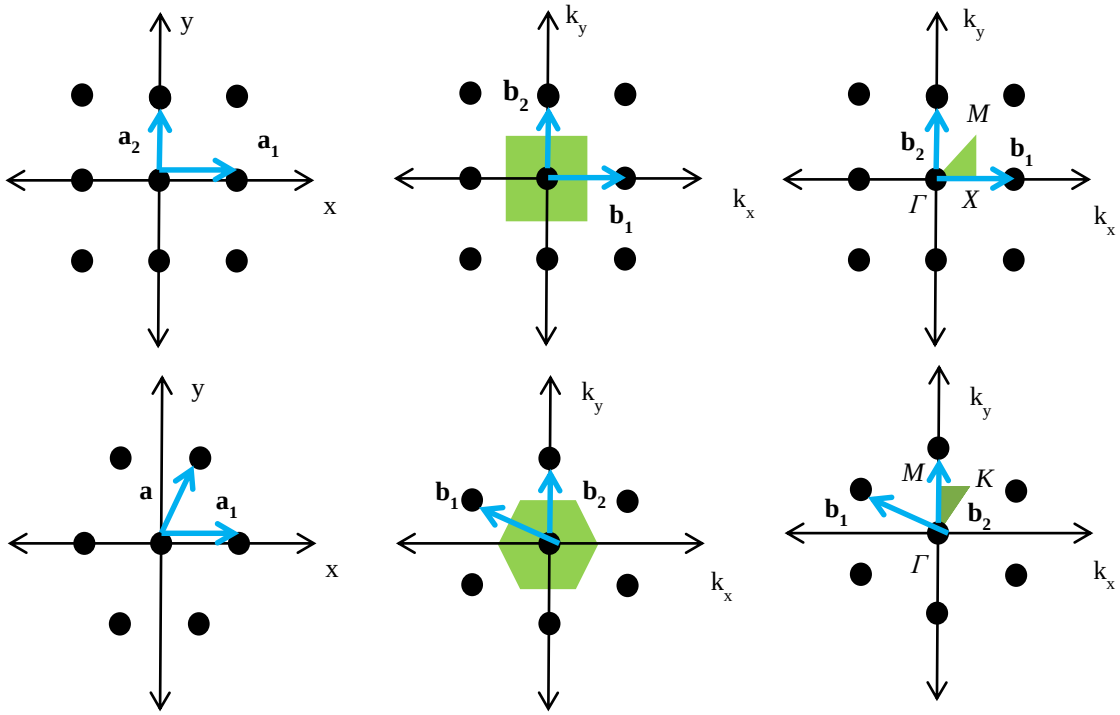

Figure 2.6: Irreducible Brillouin zone of the square and hexagonal lattice.

Chapter 3

NUMERICAL SIMULATIONS

3.1 MIT Photonic-bands (MPB)

MIT photonic-bands (MPB) software has been used for the simulation purpose [29]. It is a free tool to find eigen modes, and to compute the resonant electromagnetic modes of an infinite crystal lattice. This tool finds the modes satisfying the master equation:

$$\nabla \times [\frac{1}{\varepsilon(r)} \nabla \times H(r)] = (\frac{\omega^2}{c^2}) H(r) \qquad (3.1).$$

MPB program is a text based program and is available to run on UNIX and Linux environments. Computations for this study have been carried out on a machine with Intel core i5-3440M processor running at 2.7 GHz with installed RAM capacity of 8 GB and hosting Linux flavor named Ubuntu version 14.04.

3.2 Text Program Structure

Text program is written in a control file (with .ctl extension) and the crystal structure, geometry, number of bands (eigenvectors) to be computed are to be mentioned in the control file. In order to use the program, some definitions are required in the control file. The important definition is the specification of the primitive cell. It tells the

program that, either the crystal lattice is 1D, 2D or 3D, the information about the basis vectors, and the size of the cell in each direction. MPB solves the structure by applying discrete symmetry translation in each direction. Before writing the program, there is a need to draw the crystal real lattice and reciprocal lattice to specify k-points to the program. To minimize computational cycles, and to achieve accuracy, we should restrict k-points to the irreducible Brillouin zone. The program gives information about the k values for the specified number of bands, and the field distribution in the primitive cell either in the form of text file or HDF5 format.

3.3 Predefined Variables

MPB allows users to define variables and functions, but there are also some predefined variables, which are important, to run simulations correctly.

- **default-material –** defines the material to be used, when there is no object. Default material is air, if not mentioned by the user.
- **geometry-lattice** – defines the computational cell.
- **k-points** – are defined by the list of 3D vectors, and the corresponding eigenvalues are solved by the order of their definition. k-points are specified in the reciprocal lattice. List is empty as default.
- **num-bands** – defines number of eigenvectors to be computed at each k-point. The default value is 1.

- **resolution** – defines the computational grid size. Value can be specified as 3D vector or just a number. When specified as a number, the computational length is same in all directions, and will be different, when specified as a 3D vector. The default value is 10.

3.4 TE and TM modes

When light is propagating in the plane of periodicity, modes can be divided into two polarizations known as TE (transverse electric) and TM (transverse magnetic). Band structures can be different for TE and TM modes, and depend on the crystal structure. MPB understands the *runte* and *runtm* commands to calculate modes for TE and TM polarizations [30].

3.5 Simulation

Simulations are performed for 2D photonic crystals, for which the dielectric constant is uniform along the z-axis and varying in *x* and *y* directions. Simulations have been performed for graphite rods in air with square, hexagonal, and honeycomb lattice structures. Real permittivity ($\varepsilon = 22$) value of graphite in X-band frequencies are used for simulations [31].

3.6 Hexagonal Lattice Simulation

Circular graphite rods with radius of 0.275 cm and lattice constant of 1 cm placed in a hexagonal lattice structure are simulated in MPB. The band diagram for TE polarization is plotted in Figure 3.1.

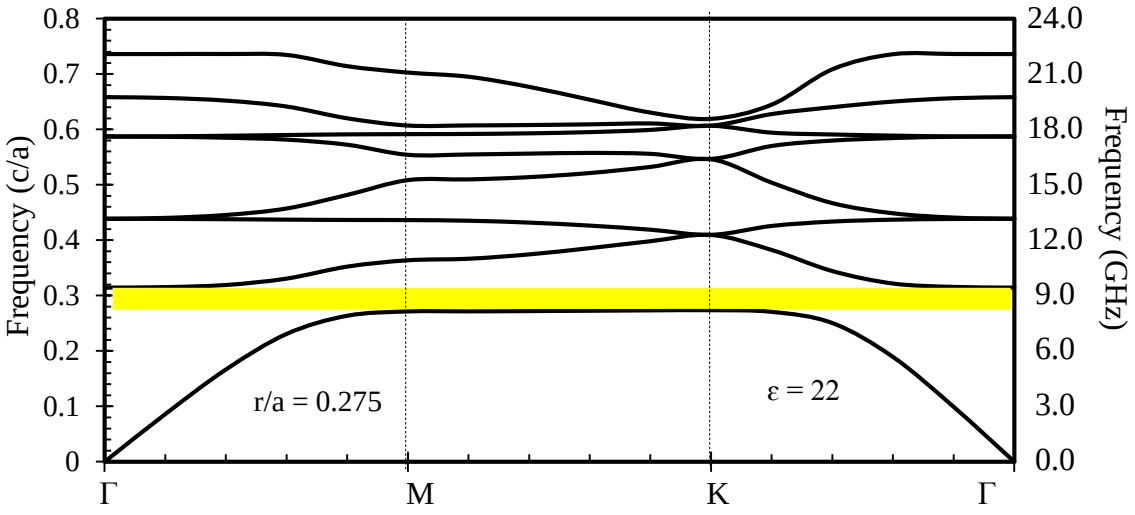

Figure 3.1: TE band diagram, bandgap shown in yellow region can be observed.

A small bandgap can be observed between normalized frequencies of 0.27 to 0.31. As mentioned before, these simulations are conducted for real permittivity. The imaginary part of permittivity is ignored, as MPB package can solve band structures for real values of permittivity. In the real scenario, because of the absorbing property of the material, no definite PBG is observed for TE polarization, and this will be discussed in Section 4.2.1.

The TM band diagram is plotted in Figure 3.2. There are three band gaps observed in the band diagrams from 0.17 to 0.25, 0.31 to 0.43, and 0.48 to 0.59 in normalized frequency values.

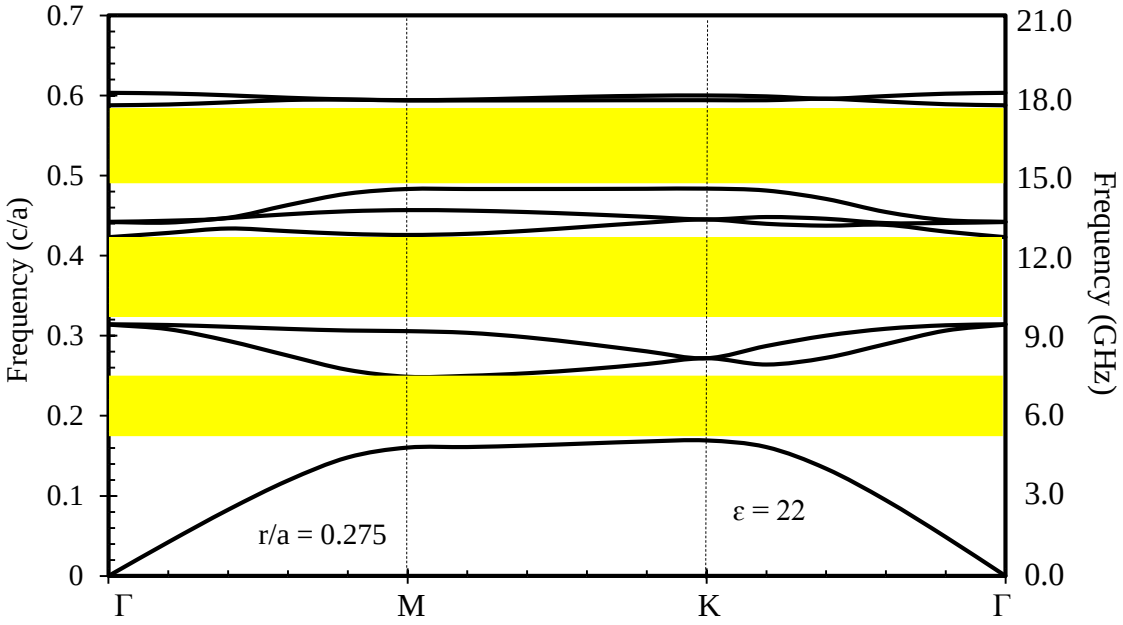

Figure 3.2: TM band diagram, bandgaps shown in yellow region can be observed.

Chapter 4

EXPERIMENTAL MEASUREMENTS

4.1 Experimental Setup

The Experimental setup for this experiment is very simple, and consists of a Network Analyzer (Agilent 8719ES) to measure the transmission spectrum (S_{21} parameter), two horn antennas, a hexagonal lattice structure, and a 360^0 rotation stage. Two ports of network analyzer are connected to two horn antennas operating in the X-band (8.2 GHz – 12.4 GHz). The antennas are shown in figure 4.1 with largest diagonal dimension of 5 cm.

The far field of antenna can be obtained at a distance:

$$r = \frac{2D^2}{\lambda} \quad ,$$

where D = 5 cm is the dimension of the antenna aperture.

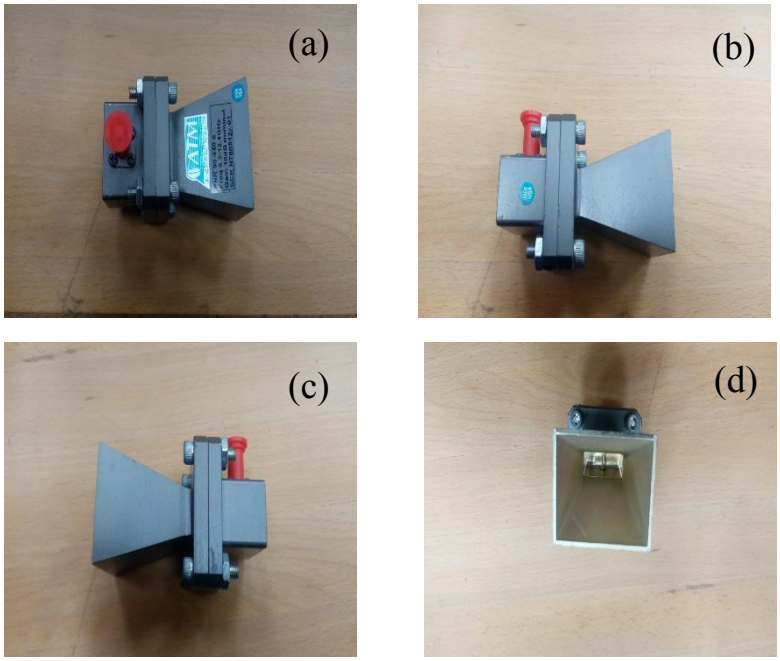

Figure 4.1: (a) Top (b), (c) side and (d) front view of horn antenna.

We have used an Agilent 8719ES network analyzer to measure S_{21} parameters. The front panel of the network analyzer is shown in Figure 4.2 (a). We can measure S_{11}, S_{12}, S_{21} and S_{22} parameters in log scale, the phase and the magnitude, and plot them in polar space, and Smith chart. The network analyzer can work in the range of 50 MHz – 13.5 GHz, but we have used it from 8.2 GHz – 12.4 due to the response of the horn antennas. A floppy disk is required to save the data. The data can be saved as snapshot or *.csv format, which can be opened in MS Excel.

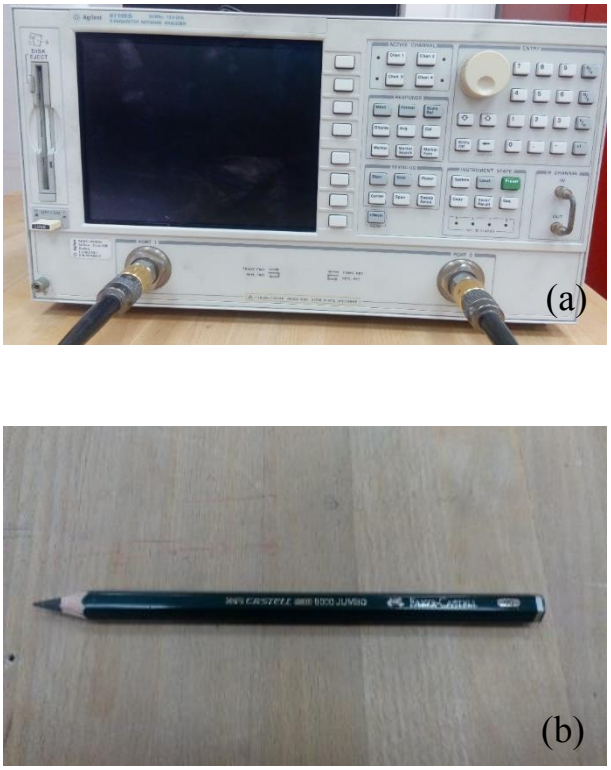

Figure 4.2:(a) Agilent network analyzer and (b) Faber Castell Jumbo pencil.

In measurement settings, every block on the vertical axis is of -10 dB value. The span of calculation is 4.2 GHz with a resolution of 5.24 MHz approximately.

The Faber Castell 9000 Jumbo pencil, used to manufacture photonic crystal, is shown in Figure 4.2 (b). The pencil shape is a hexagon so the structure easily takes the form of a hexagon, when they are stacked together. A 360^0 rotation stage is used to rotate the graphite photonic crystal structure.

The schematic of the experimental setup is shown in figure 4.3. Two horn antennas attached to the network analyzer are facing each other with the photonic crystal structure in the far field (distance between two antennas is 30 cm) of the transmitting horn and near to the receiving antenna [32].The reciprocal lattice and irreducible Brillouin zone is also represented in Figure 4.3. The antennas and photonic crystal structure is placed with the EM wave incident in the Γ-M direction.

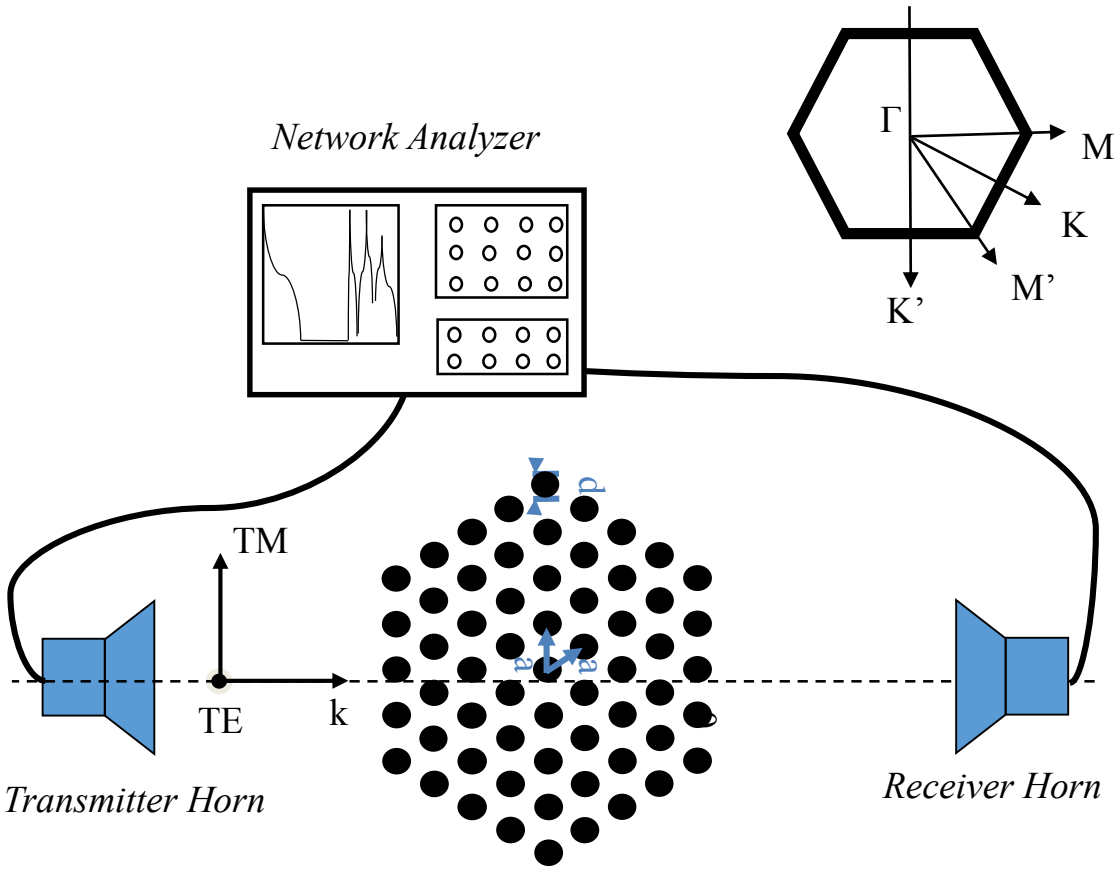

Figure 4.3: Schematic diagram of the experiment.

The real experimental environment is shown in figure 4.4. The two antennas are facing each other with the photonic crystal structure with unit cells placed on 360^0 rotation stage. The diameter of graphite rods is 55 mm and the distance between neighboring rods is 1 cm. The photonic crystal is first not included in the setup and transmission is recorded by the receiving horn. All the transmission data is in (dBs) in the thesis, and is normalized. TE and TM polarizations are defined with respect to the plane of the periodicity of photonic crystal structure. In TE case, the electric field is parallel to the rods and in the TM case the electric field is perpendicular to the rods.

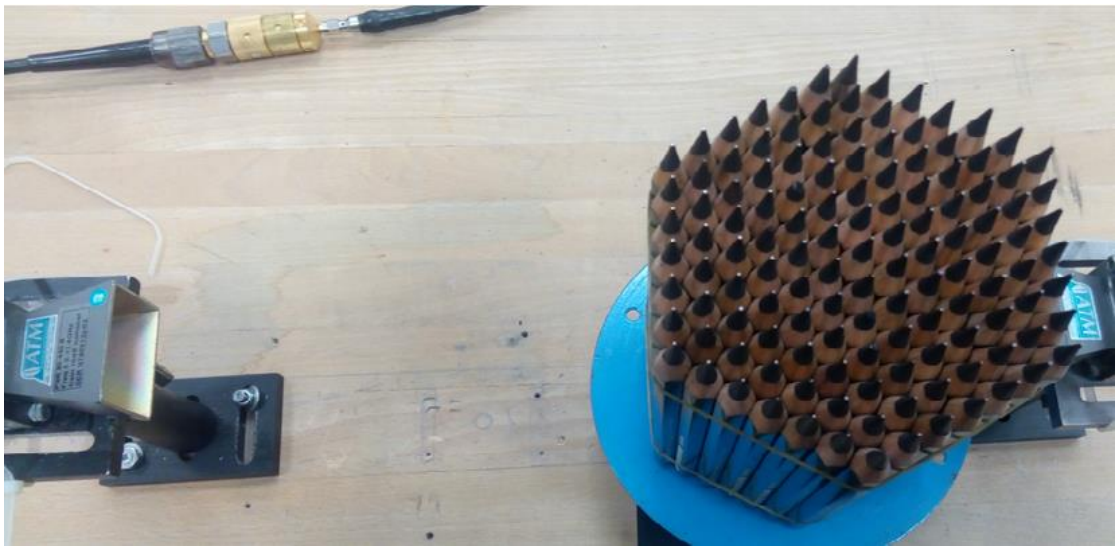

Figure 4.4: Experimental setup to measure TE transmission spectrum.

4.2 Experimental Results

4.2.1 TE Polarization

The setup shown in figure 4.4 is used to measure TE transmission spectrum from photonic crystal structure, where antennas are placed parallel to each other. The result of TE transmission through the photonic crystal structure is shown in figure

4.5. An average transmission of -45 dB is observed with no apparent structure. Graphite is an absorbing material and it is difficult to observe a bandgap due to absorbing nature of material, when the electrical field is parallel to the rods.

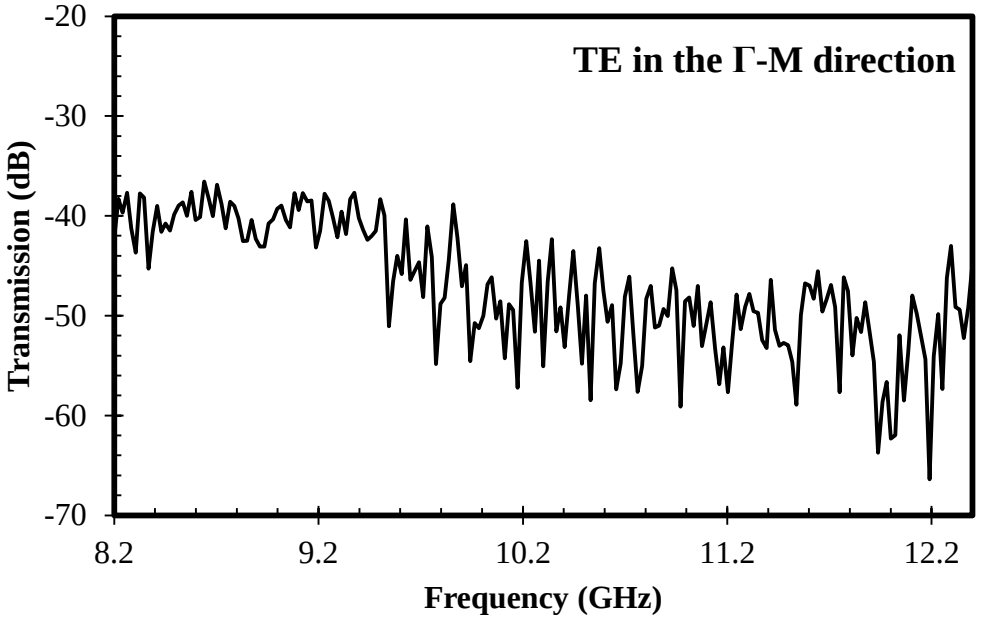

Figure 4.5: Transmission spectrum for TE polarization.

4.2.2 TM polarization

In the next step, horn antennas are fixed perpendicular to the rods to measure the TM transmission spectrum. The scenario is depicted in figure 4.6. The TM transmission spectrum is shown in figure 4.7 and a photonic bandgap can be observed. The bandgap is centered at 10.8 GHz and is 0.5 GHz wide. The transmission drops to -40 dB at the central frequency of the bandgap.

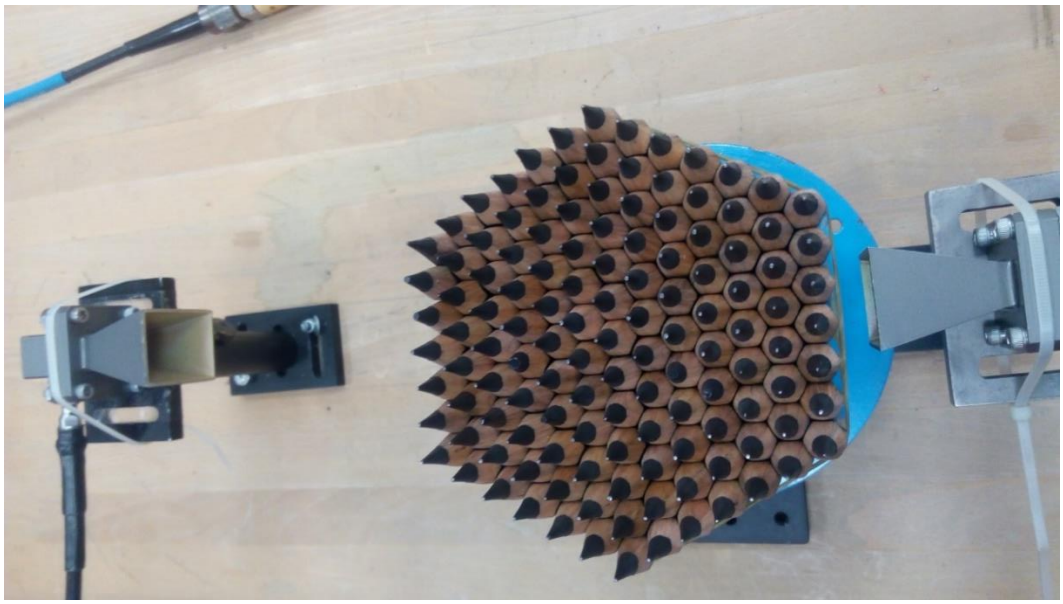

Figure 4.6: TM transmission measurement setup.

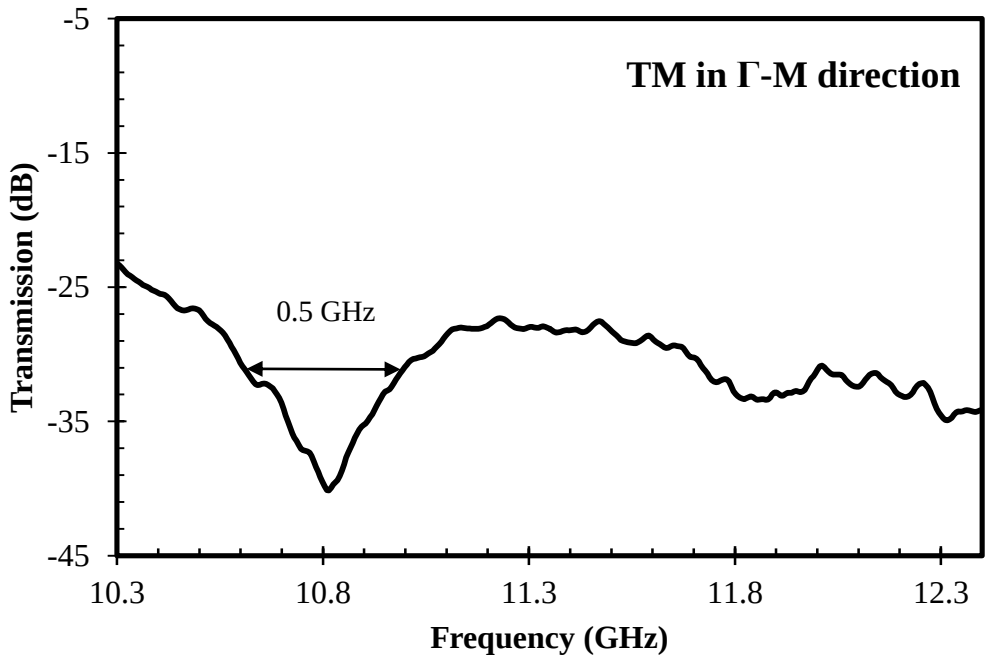

Figure 4.7: Transmission spectrum for TM polarization in Γ-M direction.

The TM transmission has an average value of -30 dB, which is 15 dB above the average value of the TE transmission. TM is not as effectively absorbed as the TE, as the TM polarization is perpendicular to the graphite rods.

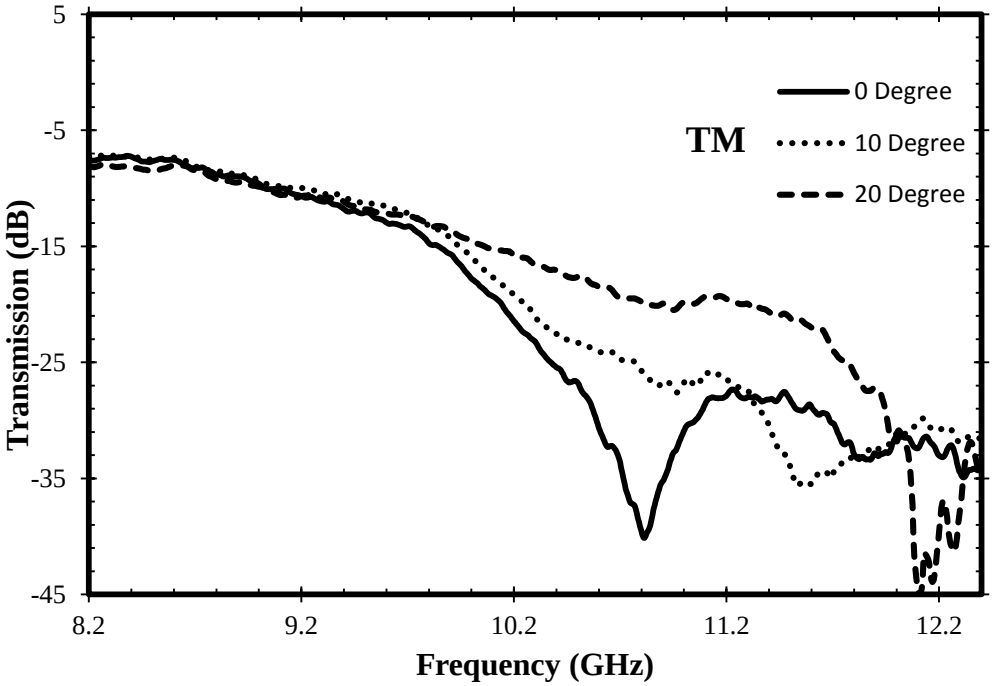

Figure 4.8: Transmission spectrum for TM for 0^o-20^o incidence angle.

The transmission spectrum with respect to change in incidence angle is plotted in figure 4.8. We can observe that, the bandgap is shifting to higher frequencies with the increase of the incidence angle. The bandgap thickness and depth are also changing with the change in the incidence angle. The bandgap width changes to 0.6 GHz at 10^0 angle of incidence, and shrinks to 0.25 GHz at 20^0 angle of incidence.

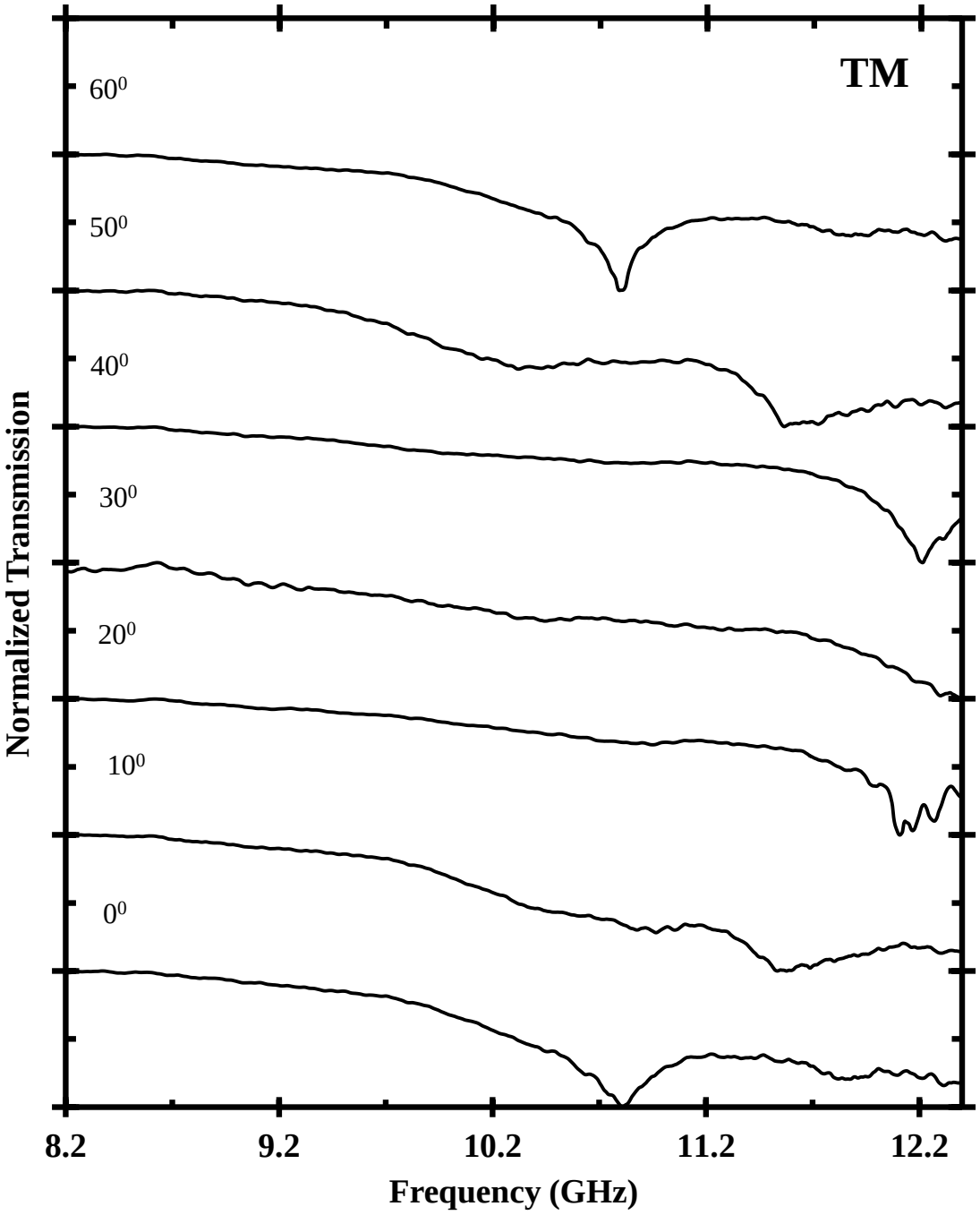

Figure 4.9: Normalized TM Transmission spectrum for 0^0-60^0 incidence angle.

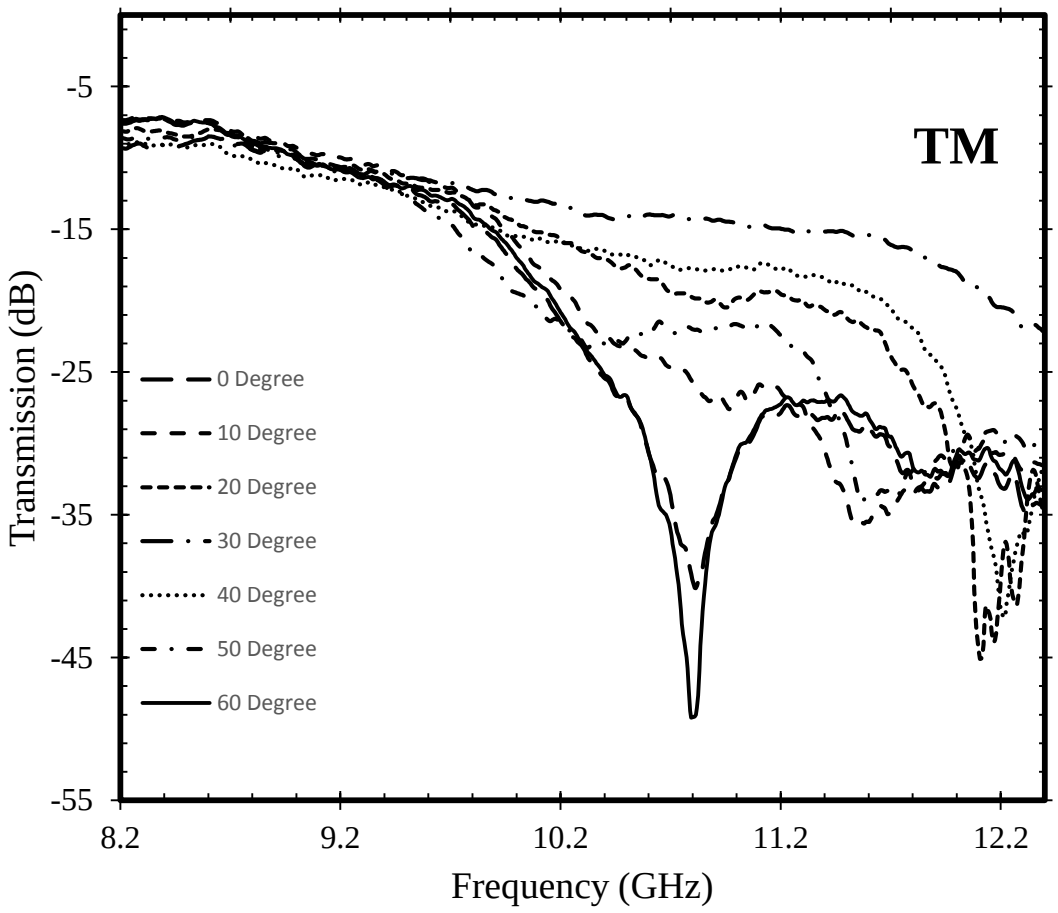

Figure 4.10: TM Transmission for 0^0-60^0incidence angle.

The transmission spectrum for TM polarization with the angle of incidence changing from 0^0 to 60^0 is plotted in figure 4.9 with normalized values, and in figure 4.10 with transmission in dB. The bandgap moves away from 0^0 to 20^0, and then no peak is observed for 30^0 in the X-band. The bandgap starts to move towards lower frequencies from 40^0 to 60^0. The shape of the transmission and the bandgap frequency is the same

at 0^0 and 60^0. The structure has 60^0 rotation symmetry, and 30^0 reflection symmetry, which are evident in the plots.

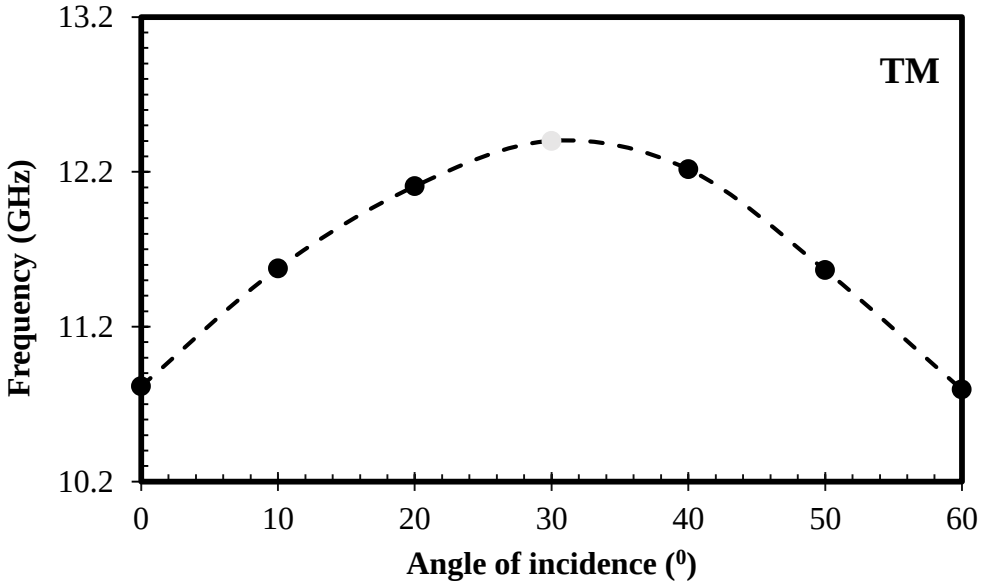

Figure 4.11: TM Bandgap frequency with respect to the incidence angle.

The TM bandgap frequency shift with change in the angle of incidence is shown in figure 4.11. We can observe a frequency shift to higher frequencies from 0^0 to 20^0. The value for 30^0 is shown at different color, because we did not observe any PBG at 30^0. The central PBG frequency shifts to lower values, as the angle of incidence increases from 40^0 to 60^0. The values are similar for 20^0 and 40^0, 10^0 and 50^0, and 0^0 and 60^0, respectively.

4.3 Defects in the Hexagonal Lattice

In the next series of experiments, we studied PC structures with defects and performed two types of experiments: one with a point defect with central rod removed, and another in which three unit cells are removed.

4.4 Point Defect in Hexagonal Lattice

Schematic of the experimental setup to measure point defect in PC structure is

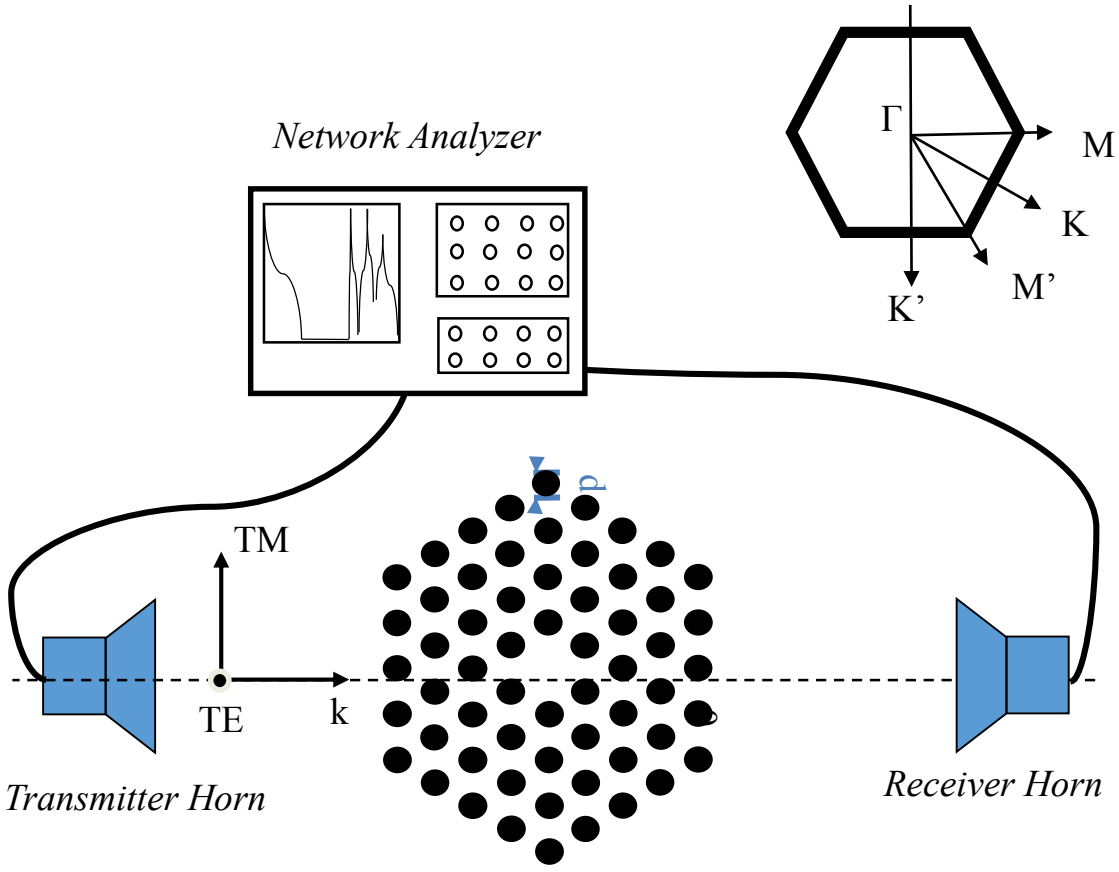

Figure 4.12: Schematic of transmission measurement of PC with point defect.

shown in figure 4.12 and the real experimental is depicted in figure 4.13, where the central rod can be observed as absent.

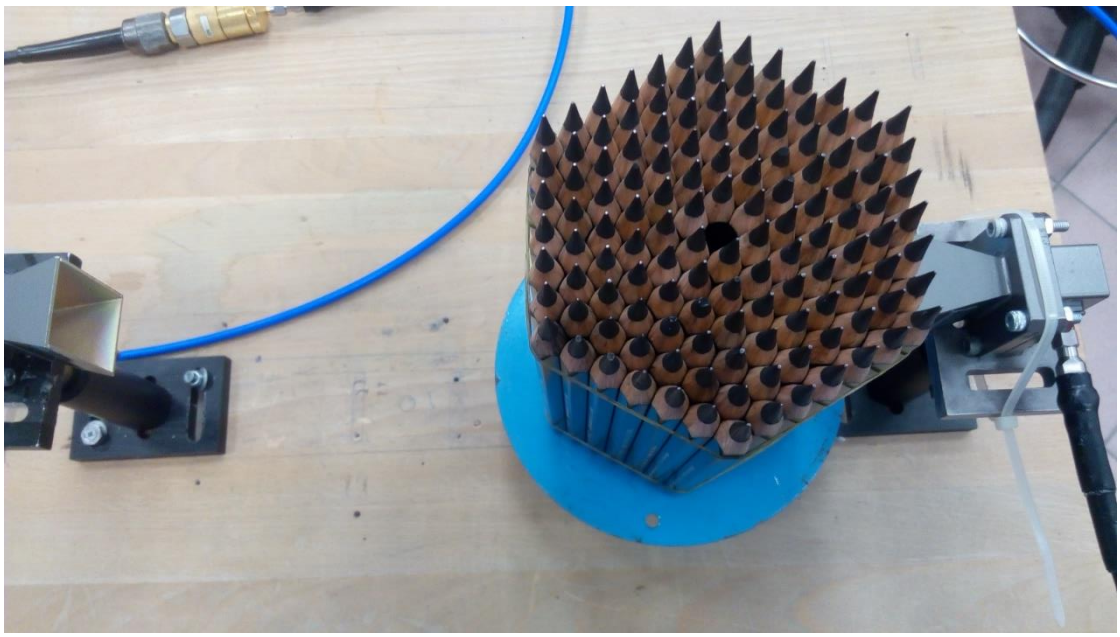

Figure 4.13: Photonic crystal with central rod removed.

The experimental results are shown in figure 4.14. A blown up image is represented in figure 4.15, where a mode in the forbidden frequency band gap is observed. The band edges of plots with defect and without defect are not coinciding because of the normalization of the data. The mode is wide because of the absorbing nature of the material and hence has a poor quality factor. This is one approach, we applied to produce a point defect. However, there are other methods to produce point defects, by varying the size of the point defect [33], or

by adding an atom with different refractive index of the central defect [34].

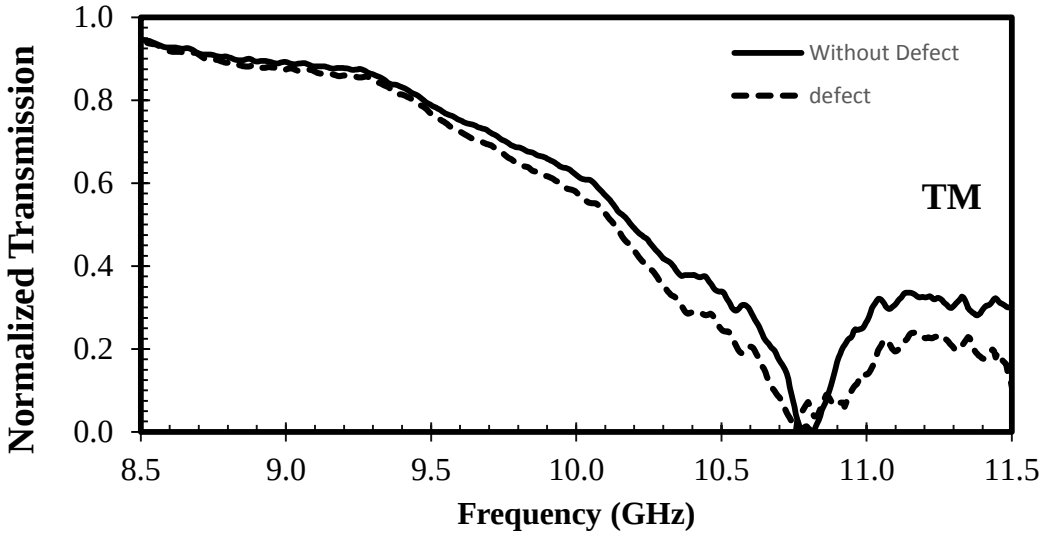

Figure 4.14: Normalized PC transmission with and without point defect.

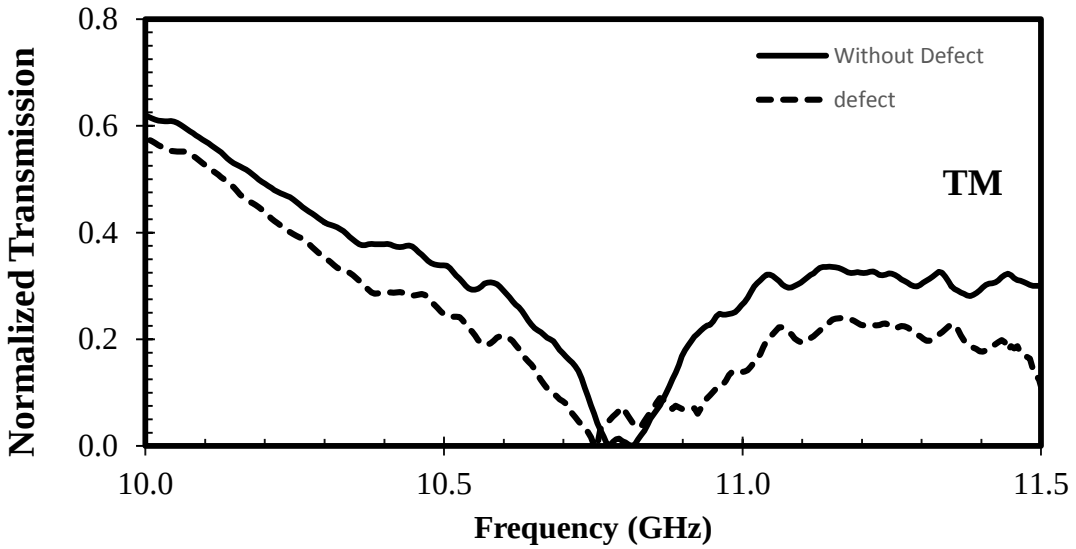

Figure 4.15: Blown up spectrum of figure 4.14.

4.5 Defect in hexagonal lattice by removing three unit cells

The schematic of the experimental setup to measure a defect in the PC structure by removing three unit cells is shown in figure 4.16, where three unit cells can be observed as absent.

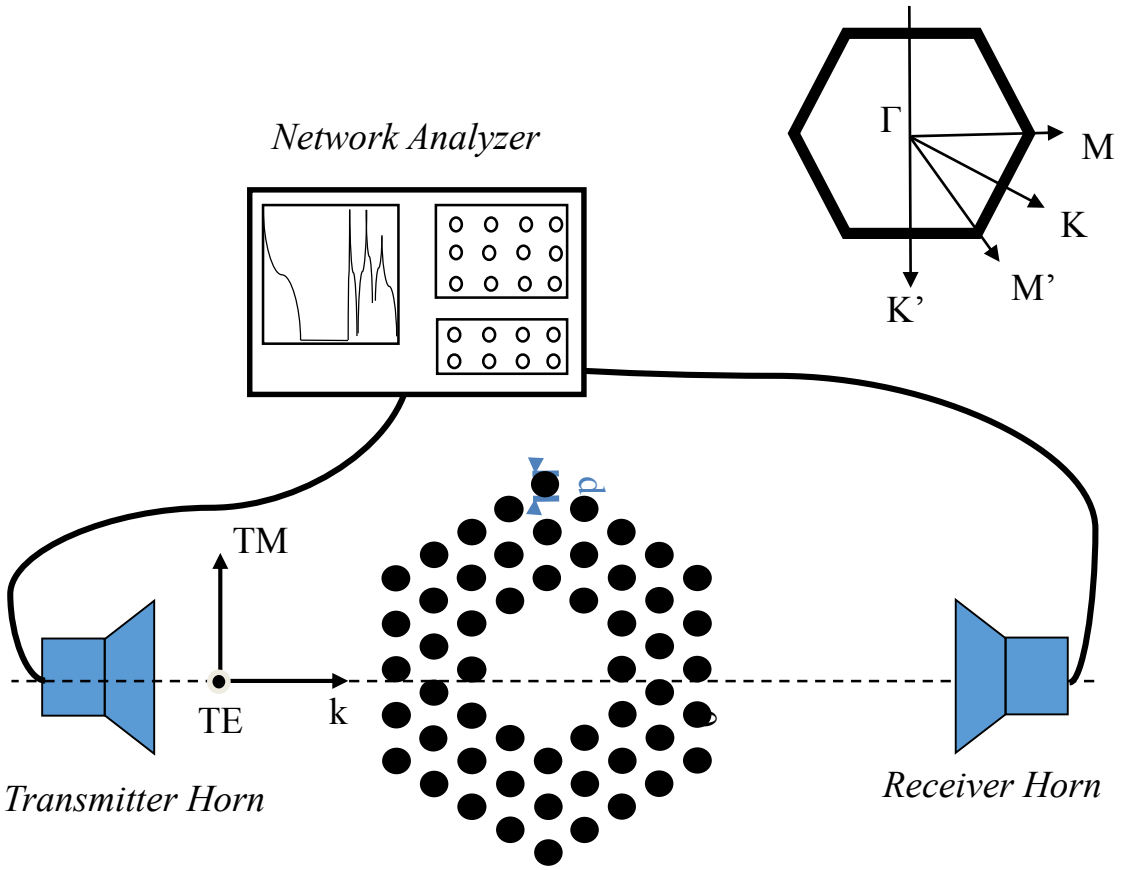

Figure 4.16: Schematic to measure PC transmission with three unit cell defect.

The experimental results are shown in figure 4.16. The central PBG frequency shifted to red by 0.25 GHz.

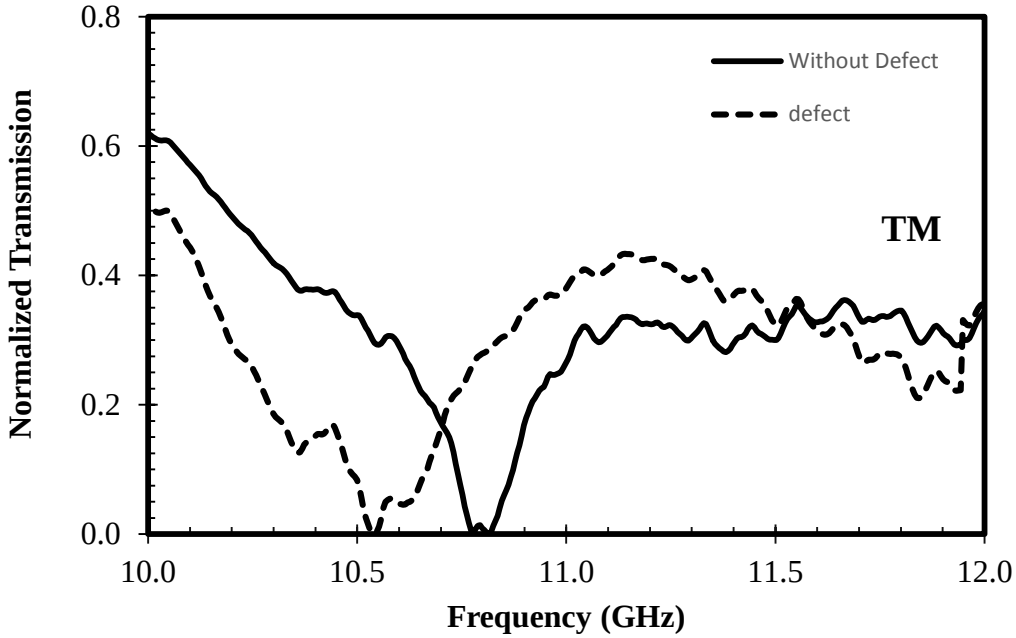

Figure 4.17: Transmission spectrum of PC with and without 3 unit cell defect.

Chapter 5

CONCLUSIONS

We measured a photonic bandgap in the microwave X-band for TM polarization in a two dimensional hexagonal lattice photonic crystal. The measured PBG is centered at 10.8 GHz and is 0.5 GHz wide. We presented our results for microwaves scattered in the 2D structure, where the scattering medium consists of circular rods of graphite, having a radius of 0.275 cm and a lattice constant of 1 cm. The photonic band gap is dependent on the angle of incidence. The transmission spectrum agrees with the reflection and rotation symmetry of the crystal structure.

We also studied defects in the hexagonal photonic crystal, and results of two types of defects are presented. First a point defect is created, by removing the central graphite rod, and we observed a mode in the forbidden frequency band. In the second experiment, we created a defect by removing three unit cells from the structure, and a red shift in the bandgap is observed.

Future experiments can involve producing line defects in the structure and to study the transmission characteristics.

VITA

Muhammad Rehan Chaudhry attended the Crescent Model Higher Secondary School, Lahore from 1991 to 2001 for his secondary school studies. He passed the higher Secondary School Exam in Pre-Engineering studies from the Forman Christian College, Lahore in 2003. Afterwards, he completed his Bachelor studies in Electrical Engineering at oldest and one of the prestigious engineering university of Pakistan, the University of Engineering and Technology, Lahore in 2007.

In 2013, he received a Higher Education Commission (HEC) of Pakistan Scholarship and chose Koç University, Istanbul for his graduate studies after getting accepted in M.Sc. Optoelectronics and Photonics Engineering program as a teaching and research assistant. He joined the Koç University Microphotonics Research Laboratory led by Prof. Dr. Ali Serpengüzel. During his study in Koç University Microphotonics Research Laboratory, he worked on elastic light scattering of a CO_2 laser from microspheres, and of microwaves from photonic crystals.

BIBLIOGRAPHY

[1] G. Keiser, “Optical fiber communications,” John Wiley & Sons, Inc. (2003).

[2] E. Yablonovitch, “Inhibited spontaneous emission in solid-state physics and electronics,” Physical Review Letters **58**, 2059–2062 (1987).

[3] S. John, “Strong localization of photons in certain disordered dielectric superlattices,” Physical Review Letters **58**, 2486–2489 (1987).

[4] D. A. Neamen, “Semiconductor physics and devices,” McGraw-Hill Higher Education (2003).

[5] C. M. Soukoulis, "Photonic band gap materials: the “semiconductors” of the future?,” Physica Scripta. **T66**, 146 (1996).

[6] A. J. Garcia-Adeva, “Band structure of photonic crystals with the symmetry of a pyrochlore lattice,” Physical Review B **73**, 073107 (2006).

[7] J. D. Joannopoulos, R. D. Mead and J. N. Winn, “Photonic Crystals: Molding the Flow of Light,” Princeton University Press (1995).

[8] K. M. Ho, C. T. Chan and C. M. Soukoulis, “Existence of a photonic gap in periodic dielectric structures,” Physical Review Letters **65**, 3152 (1990).

[9] K. Sakoda, "Optical properties of photonic crystals," 2nd ed. Berlin ; New York: Springer (2005).

[10] P. Vukusic and J. R. Sambles, "Photonic structures in biology," Nature **424**, 852-855 (2003).

[11] M. Koba and P. Szczepański, "Coupled Mode Theory of Photonic Crystal Lasers," INTECH Open Access Publisher (2012).

[12] J. D. Joannopoulos, P. R. Villeneuve and S. Fan, "Photonic crystals: putting a new twist on light," Nature **386**, 143-149 (1997).

[13] W. M. Robertson, G. Arjavalingam, R. D. Meade, K. D. Brommer, A. M. Rappe and J. D. Joannopoulos, "Measurement of photonic band structure in a two-dimensional periodic dielectric array," Physical Review Letters **68**, 2023 (1992).

[14] S. Fan, J. D. Joannopoulos, J. N. Winn, A. Devenyi, J. C. Chen and R. D. Meade, "Guided and defect modes in periodic dielectric waveguides," Journal of the Optical Society of America B **12**, 1267-1272 (1995).

[15] M. L. Povinelli, S. G. Johnson, S. Fan and J. D. Joannopoulos, "Emulation of two-dimensional photonic crystal defect modes in a photonic crystal with a three-dimensional photonic band gap," Physical Review B **64**, 075313 (2001).

[16] O. Painter, J. Vučkovič and A. Scherer, "Defect modes of a two-dimensional photonic crystal in an optically thin dielectric slab," Journal of the Optical Society of America B **16**, 275-285 (1999).

[17] L. Pavesi, L. D. Negro, C. Mazzoleni, G. Franzo and F. Priolo, "Optical gain in silicon nanocrystals," Nature **408**, 440-444 (2000).

[18] J. W. Strutt, "On the Maintenance of Vibrations by Forces of Double Frequency, and on the Propagation of Waves Through a Medium Endowed with a Periodic Structure," Philosophical Magazine., S.5 **24**, 145-59 (1887).

[19] A. Yariv and P. Yeh, "Optical waves in crystals," Vol. 10. Wiley, New York (1984).

[20] E. Yablonovitch, T. J. Gmitter, and K. M. Leung, "Photonic band structure: The face-centered-cubic case employing nonspherical atoms," Physical Review Letters **67**, 2295 (1991).

[21] J. C. Knight, T. A. Birks, P. S. J. Russell, and D. M. Atkin, "All-silica single-mode optical fiber with photonic crystal cladding," Optics Letters **21**, 1547-1549 (1996).

[22] J. G. Fleming and S. Y. Lin, "Three-dimensional photonic crystal with a stop band from 1.35 to 1.95 μm," Optics Letters **24**, 49-51 (1999).

[23] S. L. McCall, P. M. Platzman, R. Dalichaouch, D. Smith and S. Schultz, "Microwave propagation in two-dimensional dielectric lattices," Physical Review Letters **67**, 2017 (1991).

[24] K. Ohtaka, "Energy band of photons and low-energy photon diffraction, "Physical Review B **19**, 5057-5067 (1979).

[25] K. E. Sapsford, T. Pons, I. L. Medintz, and H. Mattoussi, "Biosensing with Luminescent Semiconductor Quantum Dots", Sensors **6**, 925-953 (2006).

[26] R. W. James, "The Optical Principles of the Diffraction of X-Rays," London: G. Bell and Sons (1948).

[27] C. Kittel, "Introduction to solid state physics," 8th ed. Hoboken, NJ: Wiley, (2005).

[28] H. Ehrenreich, and F. Spaepen, "Solid state physics,*"* Academic Press (2001).

[29] S. Johnson and J. Joannopoulos, "Block-iterative frequency-domain methods for Maxwell's equations in a planewave basis," Optics Express **8**, 173-190 (2001).

[30] S. G. Johnson, J. D. Joannopoulos and M. Soljačić, "The MIT Photonic-Bands Manual," Massachusetts Institute of Technology, 64 (2003).

[31] M. Hotta, M. Hayashi, M. T. Lanagan, D. K. Agrawal and K. Nagata, "Complex permittivity of graphite, carbon black and coal powders in the ranges of X-band frequencies (8.2 to 12.4 GHz) and between 1 and 10 GHz," Iron and Steel Institute of Japan International **51**, 1766-1772 (2011).

[32] J. M. Hickmann, D. Solli, C. F. McCormick, R. Plambeck and R. Y. Chiao, "Microwave measurements of the photonic band gap in a two-dimensional photonic crystal slab," Journal of Applied Physics **92** , 6918-6920 (2002).

[33] K. Inoue and K. Ohtaka, eds. "Photonic crystals: physics, fabrication and applications," Vol. 94. Springer (2013).

[34] S. E. Dissanayake and K. W. Gamalath, "Point defects in GaAs photonic crystals," International Letters of Chemistry, Physics and Astronomy **4**, 91 (2015).